Electronic Supplementary Material (ESI) for Journal of Materials Chemistry A.
This journal is © The Royal Society of Chemistry 2022

Electronic Supplementary Information

Chloride-Doping, Defect and Interlayer Engineering of Copper Sulfide for Superior Sodium-Ion Batteries

Zhonghao Pan,‡[a] Xianghua Zhang,‡[b,c] Shitan Xu,[b] Mingzheng Gu,[a] Xianhong Rui,*[b] and Xiaojun Zhang*[a]

a. Key Laboratory for Functional Molecular Solids of the Education Ministry of China, College of Chemistry and Materials Science, Anhui Normal University, Wuhu 241000, China. E-mail: xjzhang@mail.ahnu.edu.cn

b. Guangdong Provincial Key Laboratory on Functional Soft Condensed Matter, School of Materials and Energy, Guangdong University of Technology, Guangzhou 510006, China. E-mail: xhrui@gdut.edu.cn

c. School of Materials Science and Engineering, Liaocheng University, Liaocheng 252000, China.

‡Z. Pan and X.H. Zhang contributed equally to this work.

Experimental

Synthesis of CuS-NCl

The concentration of hydrate copper(II) nitrate ($Cu(NO_3)_2 \cdot 3H_2O$) (0.483 g, 2.0 mmol) and thiourea (Tu, CH_4N_2S) (0.380 g, 5.0 mmol), were added in 30 mL of a mixture solution (absolute ethanol/deionized water with a ratio of 1:3 v/v) under vigorous stirring. After totally dissolved in above solution, the solution turned from blue to transparent, and then 10 mL aqueous solution of sodium chloride (NaCl) solution was added in the transparent solution under magnetic stirring for another 20 min. While the addition of NaCl was varied to give a series of reactant molar ratios, C_R=0, 0.1, 0.2, 0.3 and 0.5 (the reactant molar ratio of NaCl:Tu was marked as (C_R). Subsequently, the mixed solution was placed in a Teflon lined autoclave (50 mL) and heated at 100 °C for 18 h. After reaction, black products were rinsed with absolute ethanol and distilled water several times, and then the products were dried at 60°C in vacuum oven overnight.

Materials Characterization

The phase purities of the samples were characterized by X-ray diffraction (Bruker D8ADVANCE) with irradiation from a Cu target (Kα, λ =0.15406 nm) under a voltage of 40 KV and current of 40 mA. The morphologies and sizes of the sample were observed by a field-emission scanning electron microscopy (FESEM, Hitachi 8100, 5 KV) and transmission electron microscope (TEM, Hitachi HT-7700, 120KV). X-ray energy dispersive spectroscopy (EDS) was obtained on FESEM. High-resolution transmission electron X-ray energy dispersive microscopy (HRTEM) images were obtained using a transmission electron microscopy (TEM, FEI TECNAI-G2 200 kV). The Brunauer-Emmett-Teller (BET) tests were determined via a surface analyzer (Micromeritics ASAP 2460). The pore-size distribution (PSD) curve was calculated by using the Barrett–Joyner–Halenda (BJH) algorithm. All the as-prepared samples were degassed at 100 °C for 6 h prior to nitrogen adsorption measurements. Laser Raman spectroscopy (Renishaw inVia). X-ray photoelectron spectroscopy (XPS)

measurements are performed on Thermo Scientific K-Alpha+ spectrometer (Thermofisher) to characterize the surface chemical composition. The source gun type of the XPS was Al Kα.

Electrochemical Measurements

The as-prepared samples as anode materials were used for SIBs to assess their electrochemical performance. 80 wt% as-prepared samples, 10 wt% Super-P, and 5% wt % carboxyl methyl cellulose (CMC), and 5% styrene butadiene rubber (SBR) in deionized water were mixed to obtain homogeneous slurry at last. The resulting mixture was then covered on Cu foil and dried at 80°C under vacuum overnight subsequently. Electrochemical experiments were performed using CR2032-type coin cells with active materials (1.5~2 mg) as the working electrode, Whatman porous glass fiber filter as separator, 1M sodium trifluomethanesulfonate ($NaSO_3CF_3$) in diethylene glycol dimethyl ether (DEGDME) as electrolyte and metallic sodium foil as the counter/reference electrodes. Also, 1 M $NaClO_4$ dissolved in ethylene carbonate and diethyl carbonate (EC: DEC = 1: 1 vol %) was used as an electrolyte for comparison. And the average areal loading of active materials in the electrode was approximately 1.0 mg cm^{-2}. Coin cells were assembled in an argon-filled glove box (Mikrouna, Super (1220/750/900). The galvanostatic discharge-charge characteristics were tested between the potentials of 0.2 and 2.6 V using a NEWARE battery tester. Cyclic voltammetry (CV, scanning rate range: 0.1-5 mV s^{-1}) and electrochemical impedance spectroscopy (EIS, frequency range: 0.01−100 kHz) were tested on a CHI 760D electrochemical workstation. All the electrochemical tests were carried out at room temperature (25°C) in the voltage range of 0.2−2.6 V. For doing ex-situ tests, the cells were discharged–charged to different voltages and dismantled in an Ar glove box. In order to avoid the influence of the copper foil on the copper signal, aluminum foil was used as a current collector during *ex-situ* tests, and the electrodes were rinsed in anhydrous DME to eliminate residual salts; the active materials were rapidly transferred into

the chambers in a few seconds. In the transfer process to ex situ test, samples were asked to minimize their time exposed to the air.

Calculation Methods

The present first-principles calculation was used to investigate the structures based on density functional theory (DFT). The Perdew-Burke-Ernzerhof (PBE) with projector-augmented wave (PAW) had been employed in our calculation, and the calculation had been carried out in the Vienna ab initio package (VASP). It is noted that the 4×4×2 K-points and 400 eV of cut-off energy was used to optimize the structure. For our structure, the convergence criterion can be described as: the self-consistent force is less than 0.05 eV $Å^{-1}$ and the difference of energy is less than 10^{-6} eV. In addition, for the Cu atoms, the U schemes need to be applied, and the U has been set as 2.1 eV. Moreover, Van der Waals (vdW) interactions were considered using Grimme's D3 dispersion with zero damping.

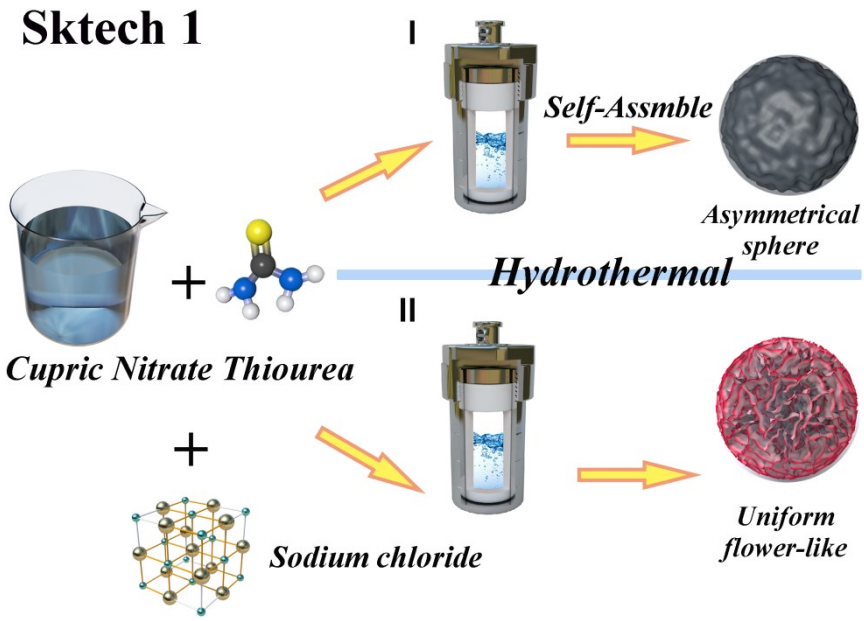

Scheme S1. Schematic diagram of the one-step synthesis process of the CuS-NCl.

The reactions of hydrate copper nitrate with thiourea (Tu) are illustrated as below.

Route I (without sodium chloride):

$NH_2CSNH_2 + H_2O \rightarrow NH_3 + H_2S + CO_2$ (1)

$Cu(NO_3)_2 + H_2S \rightarrow CuS + HNO_3$ (2)

Route II (with sodium chloride):

[Cu(Tu)]Cl clusters were formed firstly.

$Cu^{2+} + Cl^- + NH_2CSNH_2 \rightarrow Cu[NH{=}C(NH_2)\text{-}S\text{-}S\text{-}C(NH_2){=}NH]Cl$ (3)

Then, CuS-NCl was formed.

$Cu[SC(NH_2)]_2Cl + OH^- \rightarrow CuS\ (nanosheet) + NH_4^+ + CO_3^{2-} + Cl^-$ (4)

$CuS\ (nanosheets) \rightarrow CuS\ (microflowers)$ (5)

According to the above reactions, a plausible "complexation—decomposition—aggregation" mechanism is proposed for the formation of three-dimensional (3D) CuS-NCl microflowers. Specifically, it involves three stages: i) an initial complexation stage, ii) a subsequent decomposition stage, and iii) eventually the self-assembly accompanied with controlled growth of CuS-NCl.

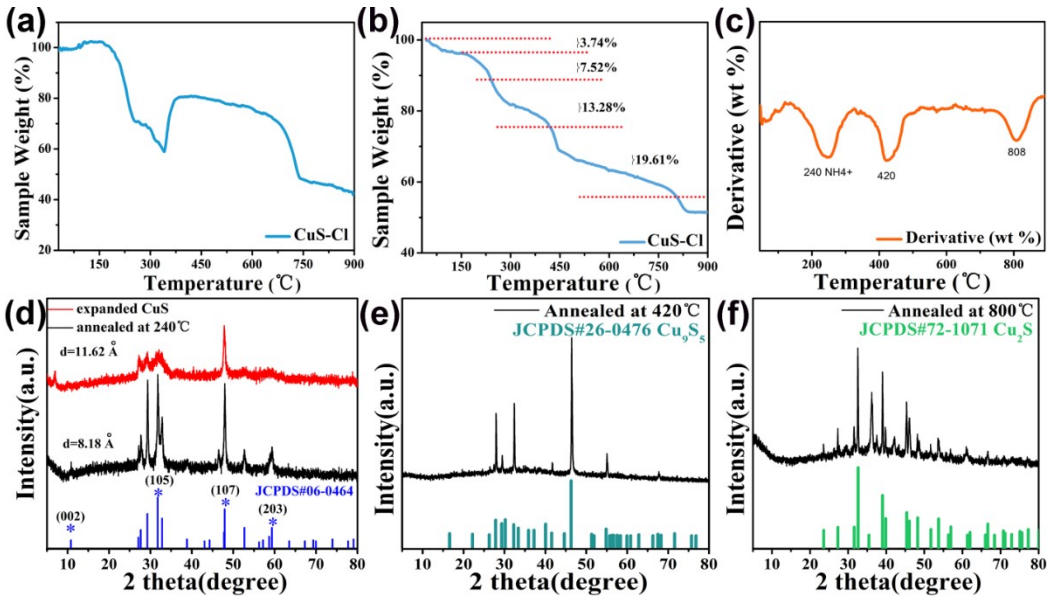

Fig. S1 TGA of CuS-NCl ($C_R = 0.3$) in (a) air and (b) inert atmosphere (N_2) at a heating rate of 10 °C min^{-1} from room temperature to 900 °C. (c) DTG curve of (b). (d-f) XRD patterns of CuS-NCl and pristine CuS annealed at 240 °C, 420 °C, 800 °C under inert atmosphere respectively.

Note: TGA curves were carried out in inert atmosphere and air to evaluate the mass content of NH_4^+ in the CuS-NCl ($C_R = 0.3$) sample. In air, it can be seen that the sample weight increases or decreases at different temperatures. The slight weight loss near 150°C results from the evaporation of water. The dramatic weight loss at around 150~340°C should be assigned to the decomposition of the unreduced ammonia-contained functional groups, and the transformation from CuS to $Cu_{1.8}S$ and Cu_2S.[1] In the next step, a sharp weight increase at around 340~420°C corresponds to the formation of $CuO{\cdot}CuSO_4$ and $CuSO_4$. Accompanied by the rising temperature above 420°C, the decomposition of $CuO{\cdot}CuSO_4$ and $CuSO_4$ leads to a further weight loss. After being heated to 740 °C, the weight of the sample becomes stable, and 43% of the original weight is left for the final product. The chemical reactions mentioned above are shown as below:

$$CuS \rightarrow Cu_{1.8}S + Cu_2S \quad (6)$$

$$Cu_{1.8}S + Cu_2S \rightarrow CuO{\cdot}CuSO_4 + CuSO_4 \quad (7)$$

$$CuO{\cdot}CuSO_4 + CuSO_4 \rightarrow CuO \quad (8)$$

Fig. S1b shows TG curve in the temperature region of 30~900°C. The weight loss below 150 °C is 3.74%, which comes from the adsorbed water. The weight has a constant value at >825 °C, and the final product is Cu_2S according to XRD result.

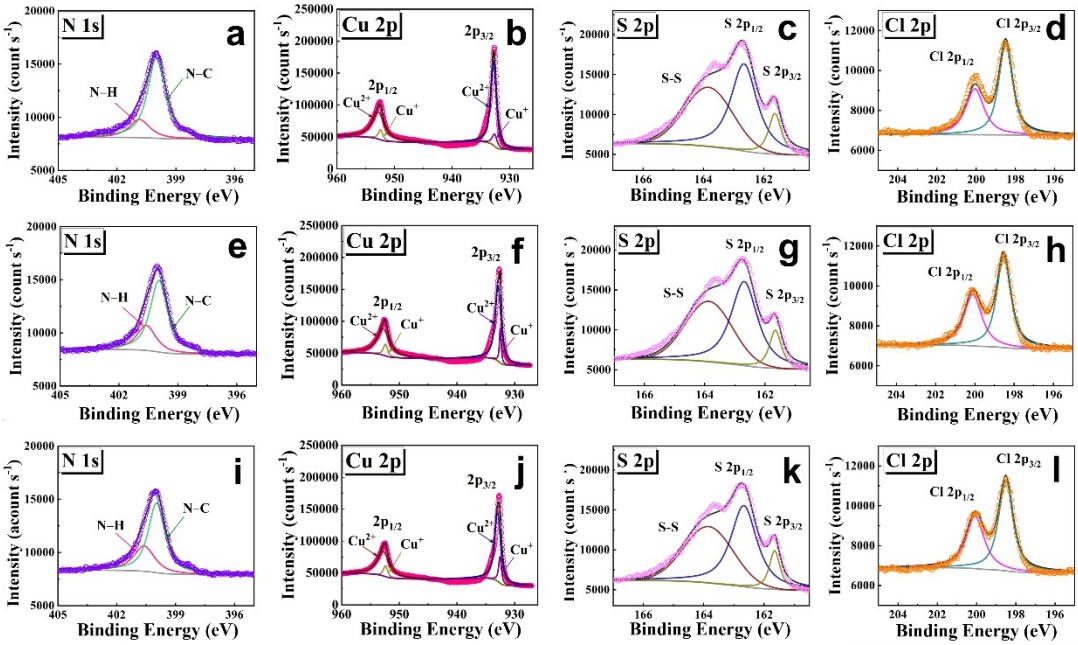

Fig. S2 XPS spectra of N 1s, Cu 2p, S 2p, and Cl 2p for samples prepared by different molar ratios of C_R = 0.1 (a-d), C_R = 0.2 (e-h), and C_R = 0.3 (i-l).

Table S1 The integral peak areas of CuS-NCl samples with C_R = 0, 0.1, 0.2 and 0.3 calculated from the XPS data in Figure S2.

Note: area unit is eV counts s^{-1}.

Element	C_R = 0.1	C_R = 0.2	C_R = 0.3
	$(NH_4)_{0.20}CuS_{0.87}Cl_{0.12}$	$(NH_4)_{0.27}CuS_{0.82}Cl_{0.16}$	$(NH_4)_{0.31}CuS_{0.78}Cl_{0.18}$
N-H	2889	3768	4143
N 1s	14335	13591	13356
S	37128	33789	31511
Cu	427793	410188	440399
Cl	5304	6492	7271

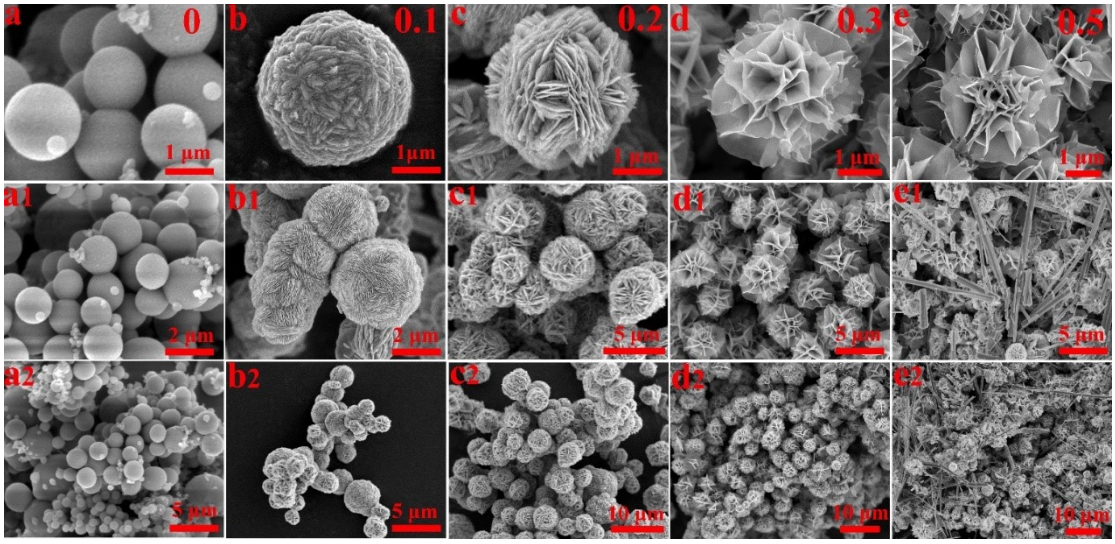

Fig. S3 SEM images of CuS-NCl samples with different molar ratios (xCl : (1-x)S) of (a, a1, a2) x = 0 (Cl : S = 0 : 1), (b, b1, b2) x = 0.1 (Cl : S = 1 : 10), (c, c1, c2) x = 0.2 (Cl : S = 1 : 5), (d, d1, d2) x = 0.3 (Cl : S = 1 : 3), and (e, e1, e2) x = 0.5 (Cl : S = 1 : 2).

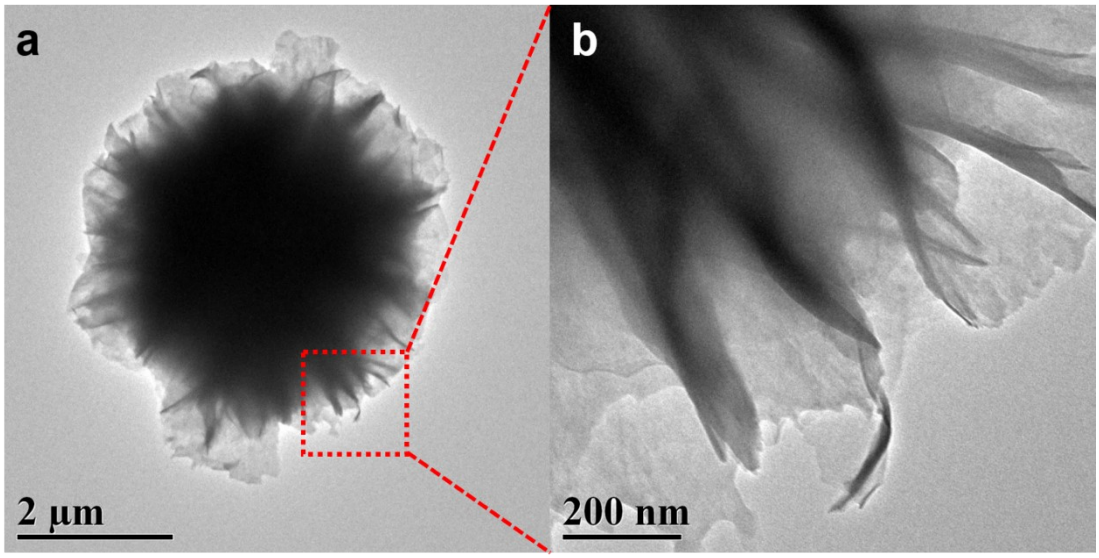

Fig. S4 TEM images of the CuS-NCl (C_R = 0.3).

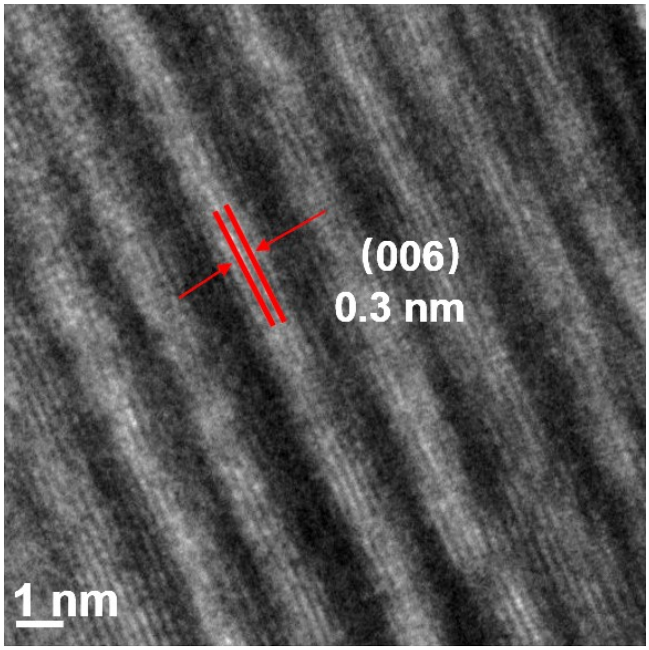

Fig. S5 Cross-section HRTEM image of the CuS-NCl (C_R = 0.3) nanosheet.

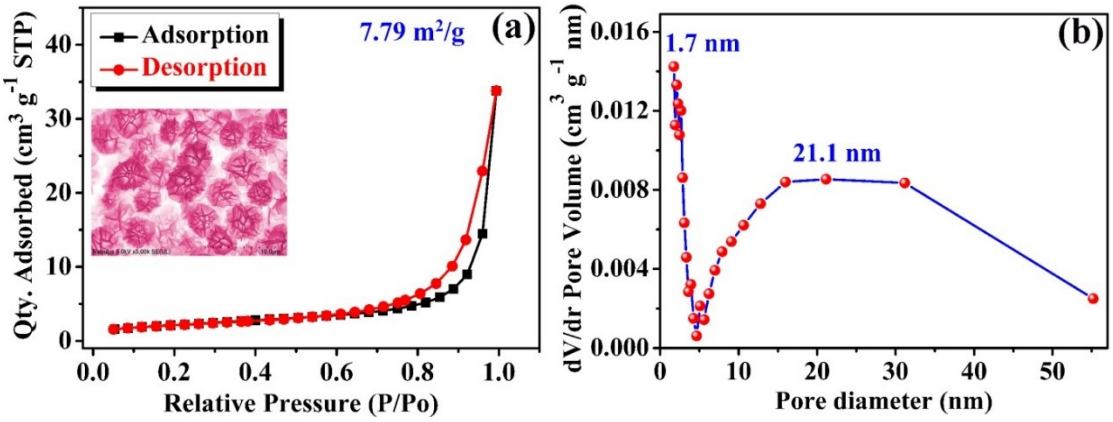

Fig. S6 (a) N_2 adsorption−desorption isotherms of the CuS-NCl (C_R = 0.3), and (b) respective BJH pore size distribution.

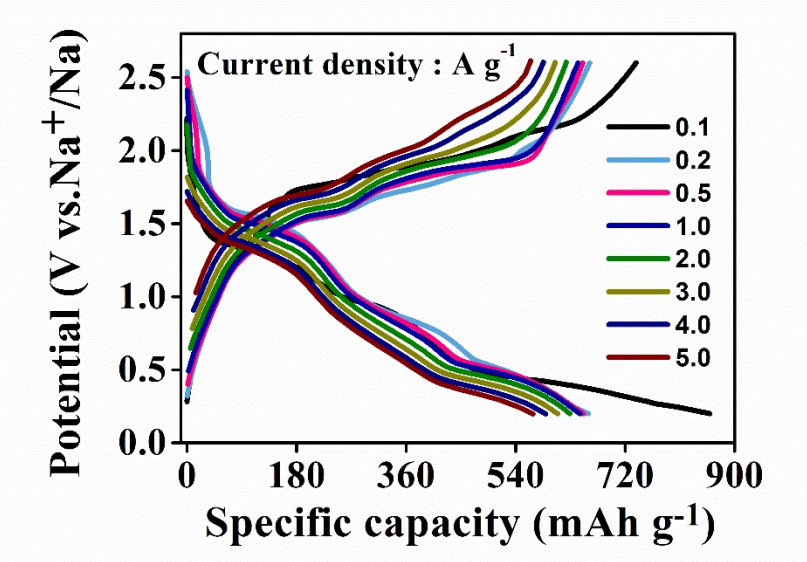

Fig. S7 Galvanostatic charge-discharge curves of the CuS-NCl (C_R = 0.3) at various rates.

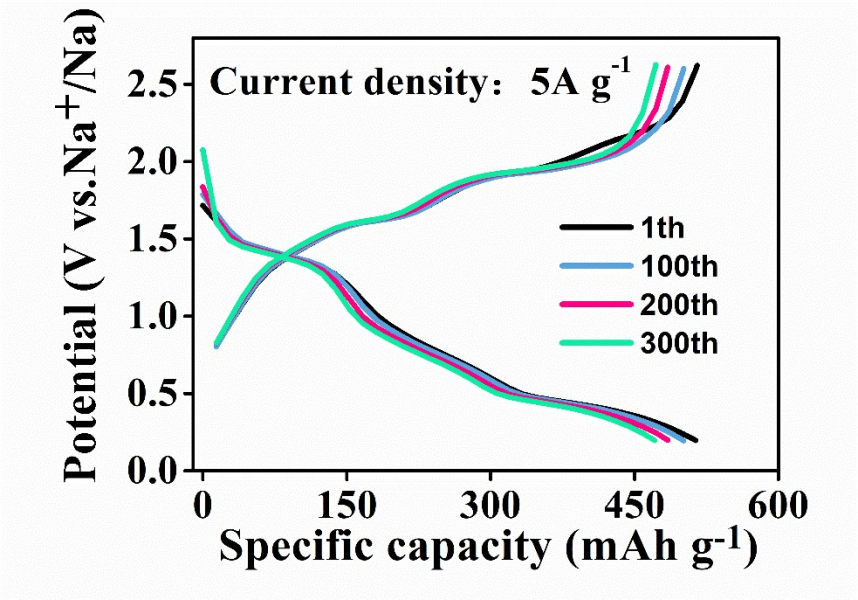

Fig. S8 Galvanostatic charge-discharge curves of the CuS-NCl (C_R = 0.3) during different cycles at 5 A g^{-1}.

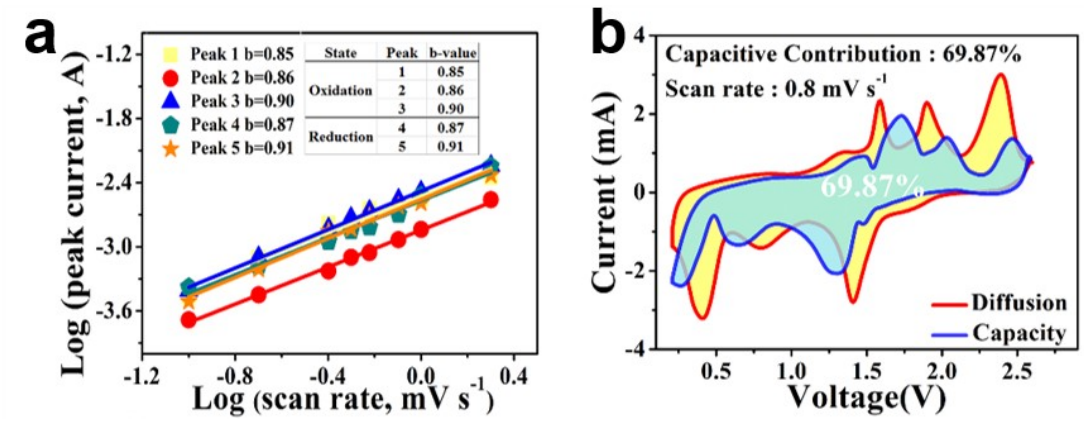

Fig. S9 (a) Plots of log(*i*) vs. log(*v*) derived from CV curves in Figure 4f. (b) Capacitive charge storage contribution at a scan rate of 0.8 mV s^{-1}.

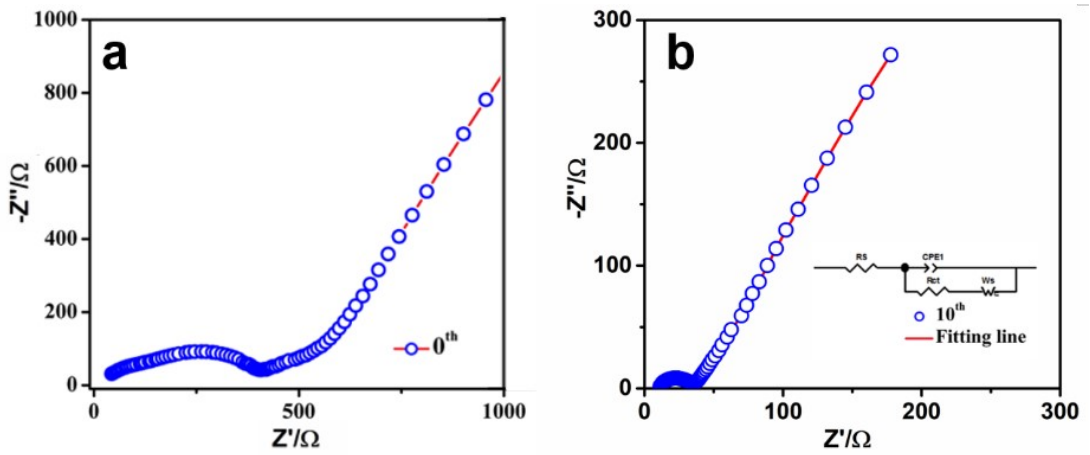

Fig. S10 Electrochemical impedance spectra of a fresh electrode (a) and after 10th cycling test (b).

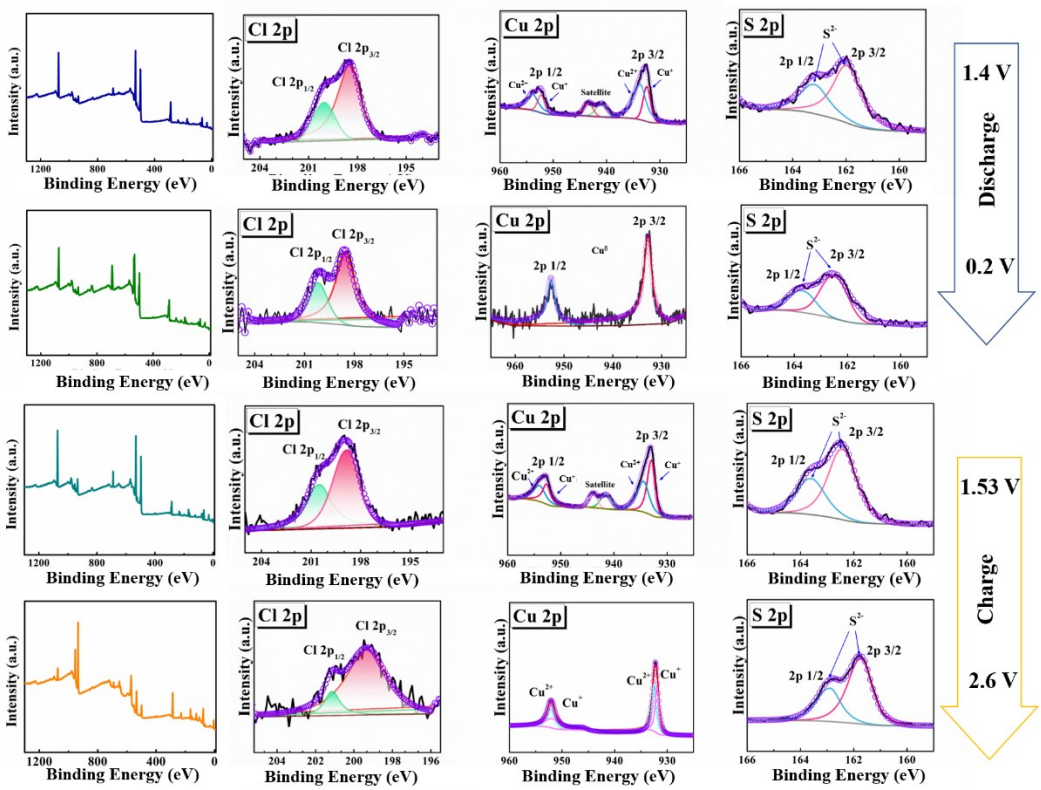

Fig. S11 The *ex-situ* XPS analysis of the CuS-NCl (C_R = 0.3) anode at various states (discharge: 1.4 and 0.2 V; and charge: 1.53 and 2.6 V).

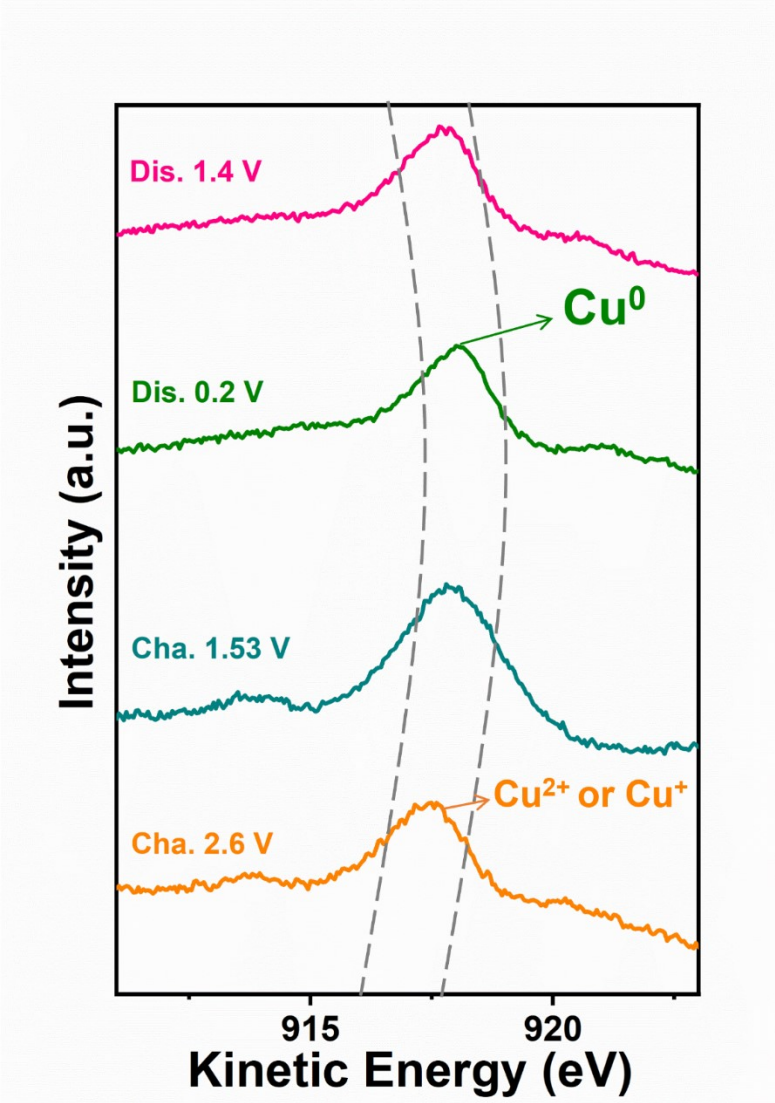

Fig. S12 The Cu LMM Auger spectra of the CuS-NCl (C_R = 0.3) anode at various states (discharge: 1.4 and 0.2 V; and charge: 1.53 and 2.6 V).

Table S2. A comparison of the rate capability of our CuS-NCl microflowers with previously reported CuS-based anodes for SIBs.

Anode Materials	Current Density	Specific Capacity	Reference
CuS-RGO	1 A g^{-1}	345 mAh g^{-1}	2
MXene/CuS hybrids	5 A g^{-1}	350 mAh g^{-1}	3
CuS microflower	5 A g^{-1}	132.6 mAh g^{-1}	4
Single-shelled CuS nanoboxes	5 A g^{-1}	206.0 mAh g^{-1}	5
CuS-NCl microflowers	**3 A g^{-1}**	**481.9 mAh g^{-1}**	**Our work**
	5 A g^{-1}	**457 mAh g^{-1}**	

Table S3. Recent progress on cupric sulfide-based anodes for SIBs.

Active Materials	Current Density	Initial Capacity	Cycles	Retention	Reference
CuS-RGO	0.1 A g^{-1}	392.9 mAh g^{-1}	50	~100%	[2]
	1 A g^{-1}	345 mAh g^{-1}	450	98%	
CuS microspheres	0.2 A g^{-1}	162 mAh g^{-1}	200	95.8%	[6]
Cu1.8S-C/C	0.1 C	372 mAh g^{-1}	110	~93%	[7]
Pine-needle-like-CuS	0.1 A g^{-1}	522 mAh g^{-1}	100	~100%	[8]
	20 A g^{-1}	317 mAh g^{-1}	1000	~58%	
CuS microflower	0.1 A g^{-1}	325.6 mAh g^{-1}	5000	~100%	[4]
	2 A g^{-1}	154.4 mAh g^{-1}	3000	~95.2%	
	5 A g^{-1}	132.6 mAh g^{-1}	5000	~100%	
Cu9S5/NSC	0.1 A g^{-1}	412.0 mAh g^{-1}	200	83.6%	[9]
CuS flower-like microsphere	5 A g^{-1}	684.9 mAh g^{-1}	100	60.4%	[10]
	10 A g^{-1}	344.9 mAh g^{-1}	1000	90.6%	
Flower-like structure CuS	0.031 A g^{-1}	348.6 mAh g^{-1}	100	12.0%	[11]
CuS-swcnt microsphere	0.1 A g^{-1}	700 mAh g^{-1}	500	42.9%	[12]
CuS-NCl microflowers	**3 A g^{-1}**	**481.9 mAh g^{-1}**	**200**	**~98%**	**Our work**
	5 A g^{-1}	**457 mAh g^{-1}**	**380**	**~100%**	

Table S4. Simulated results of EIS curves by using equivalent circuit in the inset of Figure S10.

CuS-NCl anode	R_s (Ω)	CPE (μF)	R_{ct} (Ω)
Initial state	75	38	378
The 10th cycle	11	24	36

References:

1. H. Wu, T. Li, H. Li, D. H. Zhang and F. Xu, *Mater. Lett.*, 2020, **262**, 127181.

2. J. Li, D. Yan, T. Lu, W. Qin, Y. Yao and L. Pan, *ACS Appl Mater. Interfaces*, 2017, **9**, 2309-2316.

3. P. Huang, H. Ying, S. Zhang, Z. Zhang and W.-Q. Han, *J. Mater. Chem. A*, 2022, **10**, 22135-22144.
4. C. H. An, Y. Ni, Z. F. Wang, X. D. Li and X. Z. Liu, *Inorg. Chem. Front.*, 2018, **5**, 1045-1052.

5. Y. Fang, B. Y. Guan, D. Luan and X. W. D. Lou, *Angew. Chem. Int. Ed.*, 2019, **58**, 7739-7743.
6. H. Li, Y. H. Wang, J. L. Jiang, Y. Y. Zhang, Y. Y. Peng and J. B. Zhao, *Electrochim. Acta*, 2017, **247**, 851-859.

7. C. Kang, Y. Lee, I. Kim, S. Hyun, T. H. Lee, S. Yun, W. S. Yoon, Y. Moon, J. Lee, S. Kim and H. J. Lee, *Materials*, 2019, **12**, 1324.

8. D. X. Yu, M. L. Li, T. Yu, C. Z. Wang, Y. Zeng, X. D. Hu, G. Chen, G. C. Yang and F. Du, *J. Mater. Chem. A*, 2019, **7**, 10619-10628.

9. M. J. Jing, F. Y. Li, M. J. Chen, J. H. Zhang, F. L. Long, L. M. Jing, X. P. Lv, X. B. Ji and T. J. Wu, *J. Alloy. Compd.*, 2018, **762**, 473-479.

10. Y. H. Xiao, D. C. Su, X. Z. Wang, S. D. Wu, L. M. Zhou, Y. Shi, S. M. Fang, H. M. Cheng and F. Li, *Adv. Energy Mater.*, 2018, **8**, 1800930.

11. B. Shi, W. Liu, K. Zhu and J. Y. Xie, *Chem. Phy. Lett.*, 2017, **677**, 70-74.

12. N. R. Kim, J. Choi, H. J. Yoon, M. E. Lee, S. U. Son, H. J. Jin and Y. S. Yun, *ACS Sustain. Chem. Eng.* 2017, **5**, 9802-9808.